STUDIES OF DEGENERATE FOUR-WAVE MIXING IN SODIUM, CELL AND FLAME EXPERIMENTS

DIPLOMA PAPER BY
JONAS BENGTSSON
DEPARTMENT OF PHYSICS

LRAP-95 1988

CONTENTS

ACKNOWLEDGEMENTS

I would like to thank a number of people for helping me during this diploma project. To start with, I would like to thank my supervisor, Prof. Sune Svanberg, who contributed with a great deal of help and enthusiasm. Most of all, I would like to thank Jörgen Larsson who took part in all the experiments. Finally, my thanks to everybody who helped with all whose small but still very important things.

INTRODUCTION

Early in 1977 Hellwarth proposed degenerate four-wave mixing (DFWM) as a method to create time-reversed wave fronts. This phenomenon is also referred to as optical phase conjugation [1]. Bloom and Bjorklund demonstrated the ability of image reconstruction through an aberrating medium using a four-wave mixing scheme [2]. Jensen and Hellwarth demonstrated the possibility of instantaneously generating a time-reversed replica of a monochromatic optical wave. The nonlinear medium used was CS_2 at a wavelength of 6943 Å. The demonstration illustrated image reconstruction through a distorting plate [3]. Yariv and Pepper presented an analysis of DFWM. This predicted the possibility of amplified reflection, amplified transmission, phase conjugation and oscillation [4]. One year later, Yariv presented a review on phase conjugation and DFWM [5]. This was in 1978.

All the above experiments utilized the Kerr nonlinearity of transparent materials and required high power from a pulsed laser. In 1978 Bloom, Liao and Economou presented a report on amplified reflection and self-oscillation in atomic sodium vapour. This demonstrated the possibility of enhancing the nonlinearity by using the absorbing nature of a resonance line [6]. Similar experiments were performed by Grischkowsky, Shiren and Bennet in rubidium vapour [7]. The first experiments with a continuous laser were performed by Liao, Bloom and Economou using sodium vapour [8]. Wandzura expanded the theory to include the effects of atomic motion. This was in 1979 [9].

In 1983 Bloch and Ducloy presented a theory to model the DFWM process in the case of strong optical fields. This theory explains the complex line shapes earlier obtained by others [10]. A simpler approach was presented by Grynberg, Pinard and Verkerk in 1984 [11]. This theory was later expanded [12-14].

In 1985 Pender and Hesselink reported the first observation of DFWM in a sodium-seeded flame [15]. Ewart and O'Leary reported the detection of OH in a flame using DFWM in 1986. In the same paper they reported a measurement of the sodium distribution in an sodium-seeded flame [16]. Ramsey and Whitten used DFWM as an

analytical tool in 1987. They seeded sodium, dissolved in water, into an analytical air-C_2H_2 flame. They calculated a detection limit of 10 fg/ml and obtained an experimental limit of 3 pg/ml. This resulted in an absorbance of 0.0044 for the burner used [17].

Tong and Chen used DFWM in hollow cathode discharges as an analytical spectroscopic method. They demonstrated this technique on sodium in 1987 [18].

In 1988 Ewart and Snowdon demonstrated the possibility of mapping the sodium distribution in a sodium-seeded flame using a single laser pulse [19].

In this diploma paper I will first present a short review of the theory involved. I will also describe some experiments that where performed in order to study some basic properties of degenerate four-wave mixing.

A THEORY

A1 GENERAL DESCRIPTION

In the following two sections I will try to present the theory of Degenerate Four-Wave Mixing (DFWM). The first section will give a qualitative picture which I hope will be easy to understand. The second section will deal with DFWM on a more mathematical level. It will provide quantitative results which can be compared with experimental results.

I will describe the process in terms of atomic systems. The process works, of course, just as well with molecular systems.

A1.1 ATOMIC DESCRIPTION

The geometry used in DFWM is presented by Fig. 1. The fields A_1 and A_2 are called pump waves, the field A_3 is called the probe wave and the field A_4 is the signal.

To start with, we will try to visualize the world as experienced by an atom. The atom is assumed to be stationary relative to the laboratory. When we put the atom in the situation illustrated in Fig. 1, it will experience four different fields. In a first order approach, each field will interact with the atom independently of the other fields. For each of the fields, three different processes are possible. They are absorption, stimulated emission and spontaneous emission. The overall effect of these processes is to attenuate the field and some of the power lost will appear as scattered light. The scattered light will have the same frequency as that of the incident fields and will be

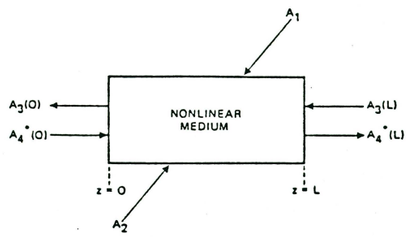

Fig. 1. The geometry used in degenerate four-wave mixing[20].

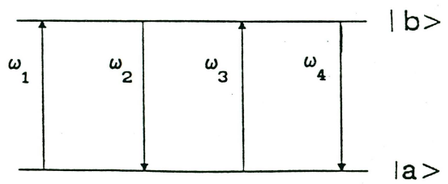

Fig. 2. The process responsible for nonlinear mixing.

uniformly distributed in all directions. This is a first order behaviour used in, for instance, laser-induced fluorescence studies. The second order behaviour, which we are interested in, consists of photons from all four fields interacting with the atom at the same time. The energy and momentum conservation laws, limiting the possible behaviour, will now only take into account the whole system of the atom and the four photons. The interaction responsible for DFWM in resonant homogeneously broadened media is illustrated in Fig. 2. One photon from each of the pump fields is absorbed and one photon is added to both the probe and signal fields by stimulated emission. Since all frequencies are equal it is obvious that energy conservation is maintained. The momentum conservation is maintained since we have two sets of counter-propagating photons and the momentum for each set cancels. The process leaves the atom in its original state. The effect on the fields is to redistribute power from the strong pump beams to the weaker probe and signal beams. In contrast to the first-order case, the power is only redistributed in well-defined directions. First-order processes are of course present simultaneously, which complicates the situation.

Another way of visualizing the process is the holographic approach. The atomic sample illuminated by one of the pump waves and the probe wave represents a real time volume hologram. The hologram is continuously read out backwards by the other pump

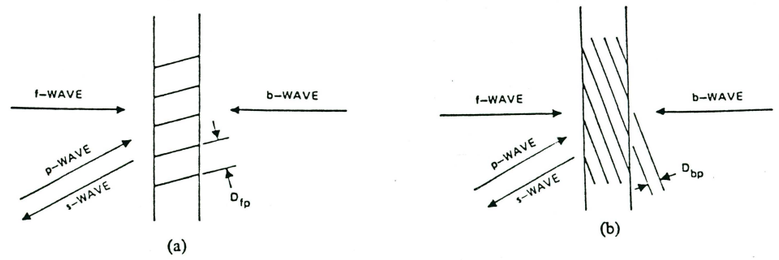

Fig. 3. Signal resulting from Bragg diffraction in volume holograms. (a) shows the signal resulting from scattering of the backward pump beam. The volume hologram is produced by interference of the other two beams. (b) shows the scattering of the forward pump beam. From [21].

wave, resulting in a signal wave which is phase conjugated relative to the probe wave. The symmetry of the system leads to a number of different holograms which are simultaneously set up and read out making contributions to the signal and probe beams. The energy originates, of course, from the reconstruction beams, i.e. the pump beams. For a person well acquainted with holographic theory all this might be obvious. I will try to clarify some of the above statements to others by the following arguments, referring to Fig 3. Suppose, for example, that the forward pump beam interacts with the probe beam. The resulting field will be spatially modulated due to interference. This spatial modulation of the intensity will induce a modulation of the refractive index due to the intensity dependence of the refractive index. The counter-directed pump beam will suffer from Bragg diffraction when passing through these planes of varying refractive index. It is possible to show that the scattered wave is counter-propagating relative to the probe wave. The same argument can be used for three more combinations of waves resulting in the same type of volume holograms that contribute power in the direction of the probe and signal waves.

A1.2 WAVE DESCRIPTION

The geometry used in DFWM was presented in Fig. 1. In this section I will try to present a theory which leads to quantitative results. This is achieved by using a formalism for the interaction of the individual fields. Most of the material is taken from [20].

Each field is assumed to be a plane wave

$$\mathbf{E}_i(\mathbf{r},t) = \frac{1}{2}\,\mathbf{A}_i(r_i)\,\exp[i(\omega t - \mathbf{k}_i\cdot\mathbf{r})] + \text{c.c.} \qquad \text{(A1.2.1)}$$

with c.c. denoting the complex conjugate. We are interested in how the weak fields A_3 and A_4 interact with the much stronger pump waves. The mixing process is degenerate in the sense that all frequencies are equal and that

$$\mathbf{k}_1 + \mathbf{k}_2 = 0\,, \qquad \mathbf{k}_3 + \mathbf{k}_4 = 0\,. \qquad \text{(A1.2.2)}$$

Using the assumption that A_3 and A_4 are nondepleted, we can derive a set of equations [20]. The starting point is the wave equation

$$\nabla^2 \mathbf{E} = \mu_0 \varepsilon_0 \frac{\partial^2 \mathbf{E}}{\partial t^2} + \mu_0 \frac{\partial^2 \mathbf{P}}{\partial t^2} \ , \qquad \text{(A1.2.3)}$$

with the polarization of the medium given by

$$\mathbf{P} = \varepsilon_0 \chi(\mathbf{E}) \mathbf{E} \ , \qquad \text{(A1.2.4)}$$

where **E** is the total field. All the important phenomena, including absorption, dispersion, four-wave mixing and saturation, are contained in the susceptibility tensor $\chi(\mathbf{E})$. The susceptibility tensor will be further discussed in section A2.

We will here consider an ensemble of two-level atoms that can be characterized by a dipole moment, μ, and longitudinal and transverse relaxation times T_1 and T_2 respectively. The meaning of these relaxation times will be further discussed in section A3. In a steady state, with all the applied fields polarized in the same direction and considering the atoms as stationary, the density matrix equations give

$$\chi(E) = - \frac{2\alpha_0}{k} \frac{(i + \delta)}{(1 + \delta^2 + |E/E_s|^2)} \ , \qquad \text{(A1.2.5)}$$

where $\delta = (\omega - \omega_0)T_2$ is the normalized detuning from line centre, $|E_s|^2 = \hbar^2/T_1 T_2 \mu^2$ is the line-centre saturation "intensity" and $\alpha_0 = \mu^2 \Delta N_0 T_2 k / 2\varepsilon_0 \hbar$ is the line-centre small-signal attenuation coefficient with $k = 2\pi/\lambda$. The total field is composed of a strong and a weak field component

$$E = E_0 + \Delta E \ , \qquad \text{(A1.2.6)}$$

where $E_0 = E_1 + E_2$ is the field from the nondepleted pump waves and $\Delta E = E_3 + E_4$ is the weak field to be calculated. The idea is to expand $\chi(E)$ about E_0 in a power series of ΔE

$$\chi(E) = \chi(E_0) + \frac{\partial \chi}{\partial E}(E_0)\Delta E + \frac{1}{2} \frac{\partial^2 \chi}{\partial E^2}(E_0)\Delta E^2 + \ . \ . \ . \qquad \text{(A1.2.7)}$$

Using the relation (A1.2.4) we can write the polarization, to first order in ΔE, as

$$P = \varepsilon_0 \chi_0 E_0 + \varepsilon_0 \chi_0 \Delta E - \frac{\varepsilon_0 \chi_0}{|E_s|^2} \frac{(E_0 \Delta E^* + E_0^* \Delta E) E_0}{(1 + \delta^2 + |E_0/E_s|^2)} \qquad \text{(A1.2.8)}$$

where $\chi_0 = \chi(E_0)$.

Using the polarization P as a source term in the wave equation (A1.2.3), we can write the propagation equations for the fields A_1 and A_2 as follows

$$\frac{dA_3}{dz} = \alpha A_3 + i\kappa^* A_4^* \quad ,$$

$$\frac{dA_4^*}{dz} = i\kappa A_3 - \alpha^* A_4^* \quad . \qquad \text{(A1.2.9)}$$

In deriving these equations the adiabatic assumption

$$\left|\frac{d^2A_i}{dz^2}\right| \ll \left|k_i \frac{dA_i}{dz}\right| \qquad \text{(A1.2.10)}$$

has been used. The equations (A1.2.9) are quite easy to interpret. The rate of increase in the field A_4^*, at every point inside the sample, is given by a negative term due to absorption and a positive term due to the coupling to the field A_3. The principle is the same for the evolution of A_3. α accounts for the saturated absorption of the weak field, in the presence of the strong field, and is given by

$$\alpha = \frac{\alpha_0}{n} \frac{1-i\delta}{1+\delta^2} \frac{1+2I/I_s}{(1+4I/I_s)^{3/2}} = \alpha_R - i\alpha_I \quad . \qquad \text{(A1.2.11)}$$

The coupling coefficient κ is given by

$$\kappa^* = \frac{i\alpha_0}{n} \frac{1-i\delta}{1+\delta^2} \frac{2I/I_s}{(1+4I/I_s)^{3/2}} \quad , \qquad \text{(A1.2.12)}$$

where κ^* is the complex conjugate of κ, $I \propto |E|^2$ is the intensity of the two equal pump waves ($I = I_1 = I_2$), $I_s \propto (1+\delta^2)|E_s|^2$ is the frequency-dependent saturation intensity and n is the refractive index including the nonlinear anomalous dispersion. The relation between α and κ is

$$\kappa^* = i \frac{2I/I_s}{1+2I/I_s} \alpha \quad . \qquad \text{(A1.2.13)}$$

For the solutions that we are interested in (see Fig. 1), we assume the complex amplitudes $A_3(L)$ and $A_4^*(0)$ to be given. In this case, the solutions of the coupled equations (A1.2.9) are

$$A_3(z) = \frac{A_3(L)\exp\left[-i\alpha_I(z-L)\right]\left(\omega\cos\omega z + \alpha_R\sin\omega z\right)}{\omega\cos\omega L + \alpha_R\sin\omega L} +$$

$$+ \frac{i\kappa^* A_4^*(0)\exp\left[-i\alpha_I z\right]\sin\omega(z-L)}{\omega\cos\omega L + \alpha_R\sin\omega L} ,$$

$$A_4^*(z) = \frac{i\kappa A_3(L)\exp\left[-i\alpha_I z\right]\sin\omega z}{\omega\cos\omega L + \alpha_R\sin\omega L} +$$

$$+ \frac{A_4^*(0)\exp\left[-i\alpha_I z\right]\left[\omega\cos\omega(z-L) - \alpha_R\sin\omega(z-L)\right]}{\omega\cos\omega L + \alpha_R\sin\omega L} \qquad \text{(A1.2.14)}$$

where $\omega = \left(|\kappa|^2 - \alpha_R^2\right)^{1/2}$. Note that if $|\kappa|^2 > \alpha_R^2$, ω is a positive real number and the functions are sinusoidal. If $|\kappa|^2 < \alpha_R^2$ then the functions are hyperbolic.

The case of interest in this study is the case of a single input, which will be called the probe wave, $A_4^*(0)$ at $z = 0$. The signal is the wave $A_3(0)$. This wave is generated within the sample, so that $A_3(L) = 0$. Equations (A1.2.14) then give

$$A_3(0) = \frac{-i\kappa^* A_4^*(0)\sin\omega L}{\omega\cos\omega L + \alpha_R\sin\omega L}$$

$$A_4^*(L) = \frac{A_4^*(0)\,\omega\exp\left[-i\alpha_I L\right]}{\omega\cos\omega L + \alpha_R\sin\omega L} . \qquad \text{(A1.2.15)}$$

The power reflection coefficient for the phase-conjugate reflected wave becomes

$$R = \left|\frac{A_3(0)}{A_4(0)}\right|^2 = \frac{\left|\kappa\sin\omega L\right|^2}{\left|\omega\cos\omega L + \alpha_R\sin\omega L\right|^2} . \qquad \text{(A1.2.16)}$$

The transmission coefficient for the incident field is given by

$$T = \left|\frac{A_4(L)}{A_4(0)}\right|^2 = \frac{\left|\omega\right|^2}{\left|\omega\cos\omega L + \alpha\ \sin\omega L\right|^2} . \qquad \text{(A1.2.17)}$$

If we examine these last two equations, we find the possibility for oscillation. In the case of ω being real, the denominator vanishes for

$$\tan \omega L = - \frac{\omega}{\alpha_R} . \qquad \text{(A1.2.18)}$$

If the medium is absorbing ($\alpha_0 > 0$), the threshold for oscillation will be in the region

$$\pi/2 < \omega L < \pi . \qquad \text{(A1.2.19)}$$

If, on the other hand, the medium provides gain ($\alpha_0 < 0$), the threshold will be in the region

$$0 < \omega L < \pi/2 . \qquad \text{(A1.2.20)}$$

When α_R increases we will reach the region where $\alpha_R^2 > |\kappa|^2$. This means that ω is an imaginary number and the oscillation condition becomes

$$\tanh |\omega| L = -\frac{|\omega|}{\alpha_R} . \qquad \text{(A1.2.21)}$$

This equation has a solution only for $\alpha_R < 0$, requiring $\alpha_0 < 0$ (gain).

The magnitude of ω is a measure of by how much the strength of the nonlinearity exceeds the absorption in the medium. It can be shown that

$$\omega = \frac{\alpha_0}{(1+\delta^2)} \frac{\sqrt{4(1+\delta^2)(I/I_s)^2 - 1}}{[\,1 + 2(I/I_s)\,]^2} . \qquad \text{(A1.2.22)}$$

For $\delta \gg 1$, ω has a maximum value for $I/I_s = 1/2$, given by

$$\omega = \frac{\alpha_0}{1+\delta^2} \frac{\delta}{4} = \frac{1}{4} \beta\delta , \qquad \text{(A1.2.23)}$$

where $\beta = \alpha_0 / (1+\delta^2)$ is the frequency-dependent small-signal field attenuation coefficient. It is often interesting to obtain the largest possible ω for the smallest attenuation coefficient, β. This is obtained by increasing the atomic density and operating far from the line centre ($\delta \gg 1$).

This section will end with some illustrations of the above theory. Fig. 4 (a) illustrates the calculated reflectivity as a function of intensity, which is normalized to the saturation intensity. The function is given for line-centre operation and for various values of the small-signal field absorption ($\alpha_0 L$). The figure tells us that for a given situation and only altering the intensity we will find a maximum for a certain value of I. If we, on the other hand, keep the intensity constant and low, the reflectivity will increase and saturate at some value of $\alpha_0 L$.

Fig. 4 (b) shows calculated reflectivity as a function of normalized intensity I/I_s for different values of the detuning (δ). The conclusion from (a) that the signal has a maximum at a certain intensity seems to be valid independent of the detuning (δ). We can also conclude that for a given value of I, the signal has a maximum for a certain non-zero value of the detuning.

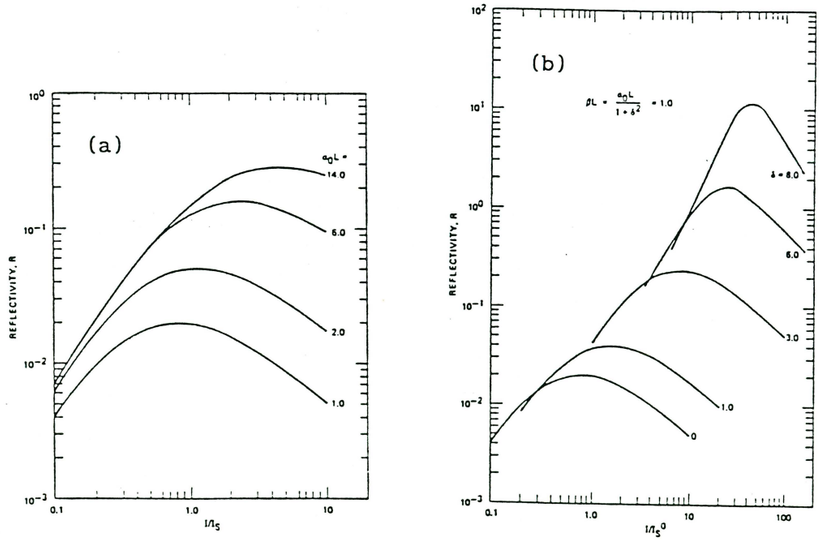

Fig. 4. Calculated reflectivity versus normalized pump intensity for various parameters. (a) is the case of line-centre operation. $\alpha_0 L$ is the small-signal field absorption. In (b) the detuning (δ) is varied for fixed small-signal absorption βL. From [20].

A2 THE SUSCEPTIBILITY TENSOR

The susceptibility tensor relates the induced polarization to the incident field. If we only consider the linear contribution the relation is

$$\mathbf{P} = \varepsilon_0 \chi\, \mathbf{E} = \varepsilon_0 \begin{bmatrix} \chi_{11} & \chi_{12} & \chi_{13} \\ \chi_{21} & \chi_{22} & \chi_{23} \\ \chi_{31} & \chi_{32} & \chi_{33} \end{bmatrix} \mathbf{E} \qquad \text{(A2.1)}$$

This implies

$$P_i = \varepsilon_0 \sum_{j=1}^{3} \chi_{ij} E_j = \varepsilon_0\, \chi_{ij} E_j \qquad \text{(A2.2)}$$

where the subscripts refer to Cartesian coordinates and the summation convention has been used in the last relation. When the incident field becomes strong enough the polarization will not be able to follow it proportionally. To describe the polarization in this case, it is possible to expand it in a series of E

$$P_i = \varepsilon_0 (\chi^1_{ij} E_j + \chi^2_{ijk} E_{jk} + \chi^3_{ijkl} E_{jkl} + \ldots) , \qquad \text{(A2.3)}$$

where the (n+1)th term is much smaller than the nth. In an isotropic medium the properties are equal in all directions. This means that if we reverse the direction of the field then the amplitude of the polarization will be the same but the sign will change. This tells us that all even order susceptibilities must be equal to zero and that the third order will be the lowest nonlinear order. The third order susceptibility tensor has, in the case of an isotropic medium, the following properties:

$$\begin{aligned} &\chi_{xxxx} = \chi_{yyyy} = \chi_{zzzz} \\ &\chi_{yyzz} = \chi_{zzyy} = \chi_{xxzz} = \chi_{xxyy} = \chi_{yyxx} \\ &\chi_{yzyz} = \chi_{zyzy} = \chi_{zxzx} = \chi_{xzxz} = \chi_{xyxy} = \chi_{yxyx} \\ &\chi_{yzzy} = \chi_{zyyz} = \chi_{zxxz} = \chi_{xzzx} = \chi_{xyyx} = \chi_{yxxy} \end{aligned} \qquad \text{(A2.4)}$$

and all other elements are zero. These four values are related, so the number of independent values is only three. The relation is

$$\chi_{xxxx} = \chi_{xxyy} + \chi_{xyxy} + \chi_{xyyx} . \qquad \text{(A2.5)}$$

In our case, where all the incident beams are polarized in the

same direction, the induced polarization will be

$$P_{NL} = 6\varepsilon_0\chi_{1111}E^3 \qquad (A2.6)$$

where 6 is a degeneracy factor.

A3 RELAXATION PHENOMENA

The DFWM process is limited by various randomizing phenomena. The motion of the free atoms tends to erase the spatial refractive index variation described in section A1.1. The internal instability of the atom limits the time available for the simultaneous interaction of four photons. In this section we will discuss the limits introduced by these phenomena.

We will start by discussing the internal behaviour of the atoms. An atom that has been transferred to an excited energy level will not remain there indefinitely. Even when the atom is left completely alone it will tend towards an energy minimum. By emitting radiation spontaneously the atom will loose energy, and finally come to rest in its ground state. In the presence of a radiation field the atom can also be stimulated to emit radiation provided that the frequency of the field corresponds to an allowed transition from the level in question. If we consider this tendency towards energy equilibrium, and only consider radiative decay, we can define a characteristic relaxation time, the longitudinal relaxation time T_1. If we, on the other hand, include all means of depopulating the given state it is common to talk of the transverse relaxation time T_2. This time is the effective relaxation time including, for example, transitions between energetically degenerate states and transitions induced by elastic collisions. Since all phenomena contributing to T_1 also contribute to T_2 it is obvious that

$$T_2 \leq T_1. \qquad (A3.1)$$

These relaxation times are not the only limit to the DFWM signal. In the case where T_1 and T_2 are very large the signal will still be limited. The motion of the atoms tends to blur the spatial modulation of the refractive index induced by the

intensity modulation. The excited atoms in the high-intensity region tend to move into the low-intensity region. This results in a steady-state condition with lower contrast in the fringe pattern than otherwise expected. The time needed for an atom to travel from one fringe to another is

$$t = d / v \,, \qquad \text{(A3.2)}$$

where d is the spacing between the fringes given by

$$d = \frac{\lambda}{2 \sin(\theta/2)} \qquad \text{(A3.3)}$$

and v is the velocity orthogonal to the fringes. If this time is much longer than all other characteristic relaxation times then the atoms can be considered as stationary.

Another limit to the strength of the fringe pattern is the time available to reach steady state. If the coherence time of the laser is shorter than all other characteristic times of the systems then the system will be given no chance to reach steady state. The coherence time is the time within which the phase of the light varies in a predictable way. This period of time is terminated by a random phase change. This phase change will appear at slightly different times in the different waves. This results in a jump in the relative phase between the waves resulting in new positions of the fringes. A completely new pattern has to be generated from scratch. A short coherence time is a problem only if it is smaller than or comparable to all other characteristic times of the system.

Fig. 5 (a) shows the reflectivity, normalized to $\delta=0$ and $\theta=0$ as a function of the detuning and for some different values of the angle θ between the probe and one of the pump beams. The function was calculated for Doppler-broadened systems. In this case, it is important to consider relaxation parameters. These are introduced according to

$$\gamma_i = \frac{1}{T_i} \frac{1}{ku} \,, \quad i = 1,2 \,. \qquad \text{(A3.4)}$$

T_1 and T_2 are the longitudinal and transverse relaxation times, respectively. ku is the Doppler width given by the wave number

$k=2\pi/\lambda$ and the thermal velocity

$$u = \left[\frac{kT}{m}\right]^{1/2}. \qquad \text{(A3.5)}$$

The values in Fig. 5 (a) are calculated for the case of $\gamma_1\gamma_2=10^{-2}$.

Fig. 5 (b) shows the reflectivity as a function of the angle θ, normalized to $\theta=0$ and $\delta=0$. The function is given for various values of the detuning and for the relaxation parameter $\gamma_1\gamma_2= 10^{-2}$.

Fig. 5 is taken from [9]. The conclusion from that reference is that at small angles the Doppler-broadened line shape will appear Doppler free. This is due to the fact that the signal originates from only one of the two holographic gratings. The distance between two maxima, d, was given in (A3.3). This equation tells us that the spacing can be very large for the grating produced by the two almost parallel beams. If the spacing is large enough, atoms will not be able to move more than a fraction of this spacing in the characteristic decay time. This means that the atomic motion can be totally neglected. This is the Doppler-free limit. In this

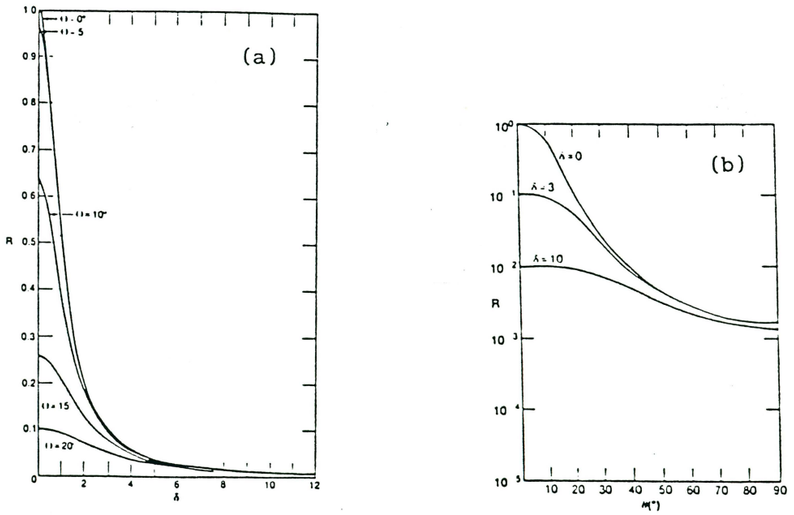

Fig. 5. Angle dependence of the reflectivity. The reflectivity is normalized and $\gamma_1\gamma_2= 10^{-2}$. From [9].

limit the functional dependence of R on δ is given by

$$R \cong \frac{\gamma_1^2\gamma_2^2}{\sin^4\theta + 16\gamma_1^2\gamma_2^2(1+\delta^2)} \frac{E_1 E_2}{E_3^2} \left[1-\exp(-2\alpha_r L)\right] . \qquad (A3.6)$$

and is found to be a Lorenzian.

A4 SATURATION PHENOMENA

This section will deal with phenomena in the high-intensity regime. The calculations presented in section A1 will no longer be valid. Instead, the concept of the dressed atom will be introduced. This results in a different line shape. Theoretical calculations are only available for the case of one strong pump beam. The dependence on which of the pump beams that is the strong one will reveal a strong anisotropy between the two cases. This is one of the fundamental aspects introduced by considering atomic motion.

In the following we will also assume that the angle between the probe beam and one of the pump beams is small. The case of the probe beam being almost parallel to the strong pump beam will be called forward saturation, whereas the opposite situation will be called backward saturation. Most of the material is taken from [12-13].

The method used to calculate the DFWM signal is as follows. The starting point is to introduce the dressed atom. When dealing with weak fields the normal procedure is to calculate the energy levels of the atom without considering the field and adding the field as a perturbation. When the strength of the field is increased this perturbation will be considerable and it will be more convenient to consider the atom and the field as one system. This is the dressed-atom approach. As will be explained below, each energy level in the dressed atom will appear as a doublet, as illustrated in Fig. 6. The energy splitting between these lines in a doublet will be $\hbar\Omega$ where Ω is the Rabi frequency. The Rabi frequency is a measure of the strength of the interaction between the field and the sample. The field connects two states in the atom. The atom will oscillate between these two states due to absorption,

stimulated emission and spontaneous emission of photons. The Rabi frequency is the frequency of this oscillation and is given by [13]

$$\Omega = \frac{d\,|E|}{\hbar} \qquad \text{(A4.1)}$$

where d is the matrix element of the electric dipole moment between the two states. For a given atom and a given field one thus considers the dressed atom as one system. This dressed atom then interacts with the weak fields, which are considered as perturbations. The possible interactions are shown in Fig. 7. An atom that is moving with a velocity v_z parallel to the direction of the beams will see the frequencies slightly shifted. These shifts are called Doppler shifts and are given by

$$\Delta\nu = \nu_0 \frac{v_z}{c} \quad \text{or}$$

$$\Delta\omega = kv_z \qquad \text{(A4.2)}$$

where ν_0 is the frequency in the laboratory frame, k is the wave number $\lambda/2\pi$ and z is the direction of the weak pump beam. The difference in frequency between the two counter-directional beams with identical ν_0 will appear to be

$$2\Delta\omega = 2kv_z. \qquad \text{(A4.3)}$$

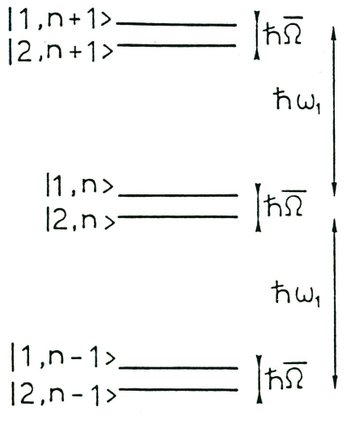

Fig. 6. Energy diagram of the dressed atom. From [13].

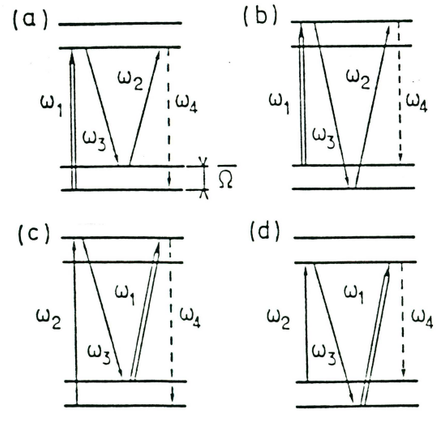

Fig. 7. Resonant DFWM in the dressed-atom energy diagram. From [13].

When this difference matches the Rabi frequency a resonance condition will be fulfilled. This resonance is called a Raman resonance. This situation is, in fact, the same as in non-resonant four-wave mixing for stationary atoms. This condition appears as a resonance denominator for the electric dipole moment in the system applied in the rotating wave approximation [13]. The resonance condition is then

$$2kv_z = \pm\bar{\Omega} \quad \text{with}$$
$$\bar{\Omega} = (\Omega_1^2 + \delta^2)^{1/2}. \qquad \text{(A4.4)}$$

In the laboratory frame we will find the following resonance velocities

$$kv_z = \frac{-\delta \pm (3\Omega_1^2 + 4\delta^2)^{1/2}}{3}. \qquad \text{(A4.5)}$$

For this perturbed atom one calculates the dipole moment in each point in space as a function of velocity. The total dipole moment for the ensemble of atoms is then obtained by integrating over the velocity distribution. The amplitude of the total dipole moment is thus given by

$$\hat{\mathcal{D}}_{pc} = \int \hat{D}_{pc}(v_z) N(v_z)\, dv_z,$$
$$N(v_z) = \frac{N}{k\sqrt{\pi}} \exp\left[-\frac{v_z^2}{u^2} \right]. \qquad \text{(A4.6)}$$

The dipole moment then gives the electric field strength, which gives the intensity. By varying the detuning (δ) and performing the above calculations one obtains the theoretical line shape.

This calculation has been done by P. Verkerk et al. [13] and G. Grynberg et al. [12]. The beams are numbered 1, 2 and 3 for the intense pump, weak pump and probe beam, respectively. The calculations are performed under the restrictions that the natural width Γ is smaller than the Rabi frequency Ω_1 for the intense beam, which is assumed to be smaller than the Doppler width ku

$$\Gamma < \Omega_1 < ku. \qquad \text{(A4.7)}$$

The Rabi frequencies of the weak beams are considered small

compared with the natural width

$$\Omega_2,\ \Omega_3 < \Gamma\ . \qquad \text{(A4.9)}$$

The calculations have been performed for both forward and backward saturation, as illustrated in Fig. 8.

The main difference between the non-saturated and the saturated line shape is that the latter is a doublet. This is due to the fact that the signal at the line centre is the sum of two resonant contributions from velocity groups with the same absolute velocity but different directions. These velocity groups induce electric dipole moments of the same magnitude but with opposite signs. The total dipole moment is thus zero. For a non-zero detuning this symmetry is removed, as seen in (A4.5) and a net dipole is induced.

In the limit of $\Omega_1 \ll ku$ the resonance occurs for a velocity much less than the thermal velocity. This means that the exponential in (A4.6), which is called the Boltzmann factor, is a slowly varying function and is approximately equal to 1 at resonance. The dipole moment varies much more rapidly and can be approximated by a delta function at each resonance point. This is the infinite Doppler-width limit. Although it might be tempting to

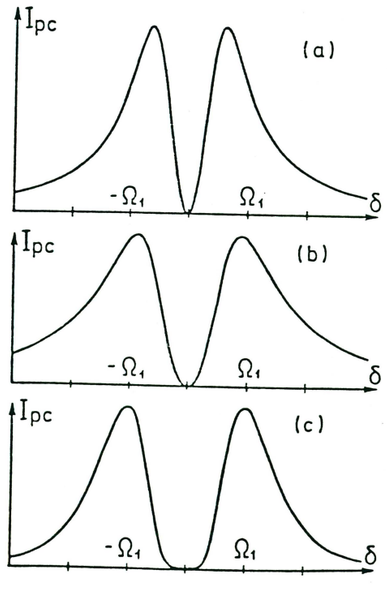

Fig. 8. Theoretical lineshapes in the saturating case. (a) is the case of infinite Doppler width and backward saturation. (b) also illustrates infinite Doppler width but for forward saturation. (c) is the case of a Doppler-free medium. These curves appear to be similar but it should be noted that their intensities can be quite different. From [12].

apply a static-atom model in this limit, since the resonance velocity is small, the above argument shows the importance of the atomic motion in tuning into resonance. This may boost the signal by several orders of magnitude. The ratio between the asymptotic intensity in the case of infinite Doppler width and the case of small Doppler width is

$$\frac{I_{inf}}{I(ku<\Omega_1)} = \frac{\Omega_1^4}{\Gamma^2 (ku)^2} \quad . \qquad (A4.10)$$

This ratio can be much larger than 1 since both the natural width and the Doppler width are smaller, and sometimes much smaller than the Rabi frequency. Theories assuming motionless atoms lead to non-resonant processes in the saturating case. In order to obtain resonance in this case the Rabi frequency must be smaller than the natural width of the lines. Fig. 8 illustrates the difference in line shape between these two cases.

If the resonance velocity is of the same magnitude as the thermal velocity, it is important to include the Boltzmann factor in the integration. The magnitude of the resonant contributions will then decrease. Fig. 9 illustrates the line shape for different ratios of Ω_1 / ku. The dashed line, which corresponds to $\Omega_1 / ku = 10^{-2}$, does not differ very much from the infinite Doppler width limit. The full line corresponds to $\Omega_1/ku = 0.25$. In this region the resonance velocity is almost of the same order as the thermal velocity. This results in a Boltzmann factor of less than

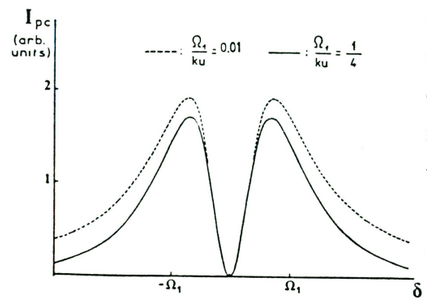

Fig. 9. Influence of the Doppler effect on the signal in the case of backward saturation. The dashed line does not differ very much from the infinite Doppler-width limit. The full line is in the region where the Doppler effect must be considered. From [13].

one. This will change the line shape since the effect is larger for larger detunings, as indicated by (A4.5).

As the resonant velocity becomes much larger than the thermal velocity ($v_z \gg u$) the resonant contribution to the total signal will decrease and finally be negligible. This is the limit that is equivalent to a motionless-atom model. The signal is non-resonant.

When looking at the dependence on Ω_1 for the two different cases of forward and backward saturation, one may observe a very interesting anisotropy, illustrated in Fig. 10. The reflectivity in the backward case is an increasing function that tends towards an asymptotic value. In the forward case, on the other hand, the reflectivity reaches a maximum and then tends towards zero. The intensity ratio between the two cases is

$$\frac{I_b}{I_f} = \frac{\Omega_1^2}{\Gamma^2} \,. \qquad \text{(A4.11)}$$

This ratio is an increasing function of Ω_1, at least as long as the limitation $\Omega_1 \ll ku$ is valid.

The above discussion concerns the special case when only one of the pump beams saturates the media. The other two beams are

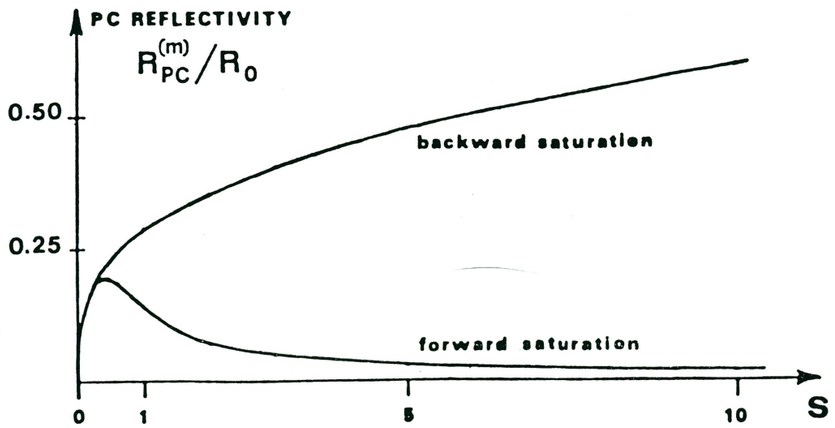

Fig. 10. Peak reflectivity versus saturation $S \propto \Omega^2$. A fundamental difference between forward and backward saturation is evident. R_0 is the asymptotic value for infinite backward saturation. From [10].

assumed to be weak, that is

$$\Omega_1,\ \Omega_2 < \Gamma\ . \qquad \text{(A4.12)}$$

Within the present theory it is not possible to explore the case of both pump beams being strong. This could be a serious limitation since the process requires that one photon is absorbed from each of the pump beams. The limited number of photons in the weak pump beam places an upper limit on the number of photons in the signal. In [12] the theory is extended to the case of $\Omega_2 \geq \Gamma$ but with the limitation $\Omega_2 \ll \Omega_1$. The result is illustrated in Fig 11. This figure illustrates the case of strong backward saturation and three different values of Ω_2/Γ. Fig. 11 (d) illustrates the emitted intensity as a function of the ratio

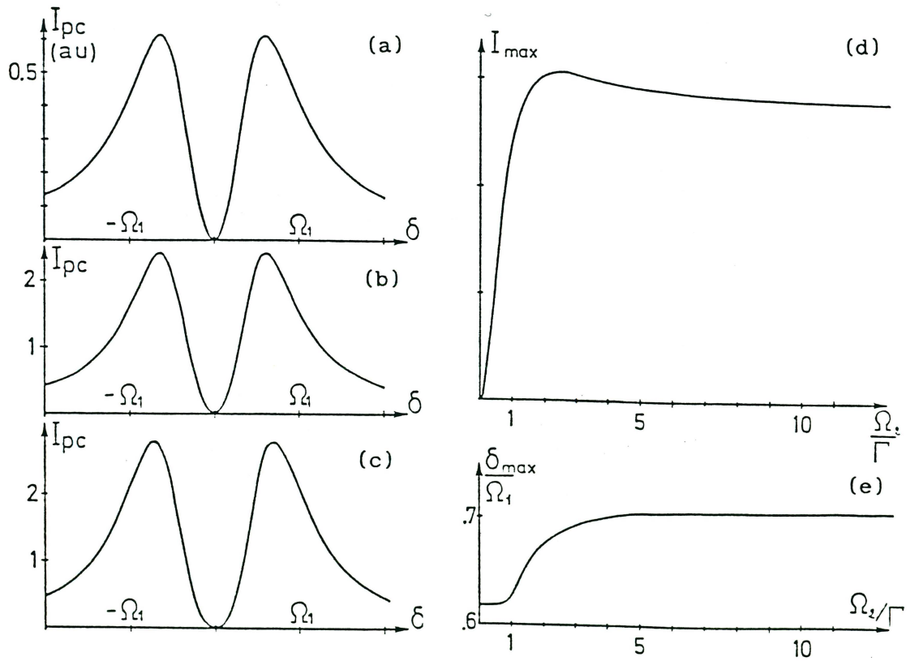

Fig. 11. Saturation by the weak beam in the case of strong backward saturation for a Doppler-broadened line. (a) to (c) are line shapes for different values of Ω_2/Γ : (a) 0.1, (b) 1 and (c) 10. (d) illustrates peak intensity versus Ω_2/Γ, and the detuning (δ_{max}) corresponding to peak intensity is given in (e). From [12].

time of this diploma work the Ar^+ laser was degrading and finally broke down completely. The maximum tunable power available was about 200 mW. When dealing with sodium this represents a high power. The only experiment requiring more power was the demonstration of phase conjugate imaging. This demonstration was therefore performed after a new plasma tube had been installed. The power used for this was about 800 mW.

A 7.5 GHz Fabry-Perot interferometer was used to check the single-mode operation of the dye laser. It was scanned piezo electrically and the transmission, which was measured by an internal photodiode, was fed to an oscilloscope.

A 50 MHz free-spectral-range Fabry-Perot interferometer was used as a wavelength reference. The transmission was measured with a diode and was fed to one of the channels on a strip-chart recorder.

The following section will be a step by step guide of how to set up the experiment and how to find the DFWM signal in a sodium sample. The first step is to make the lasers operate well. This is a matter that will not be discussed further here. The pump beams are the "ring" defined by BS5, M2 and M3 in Fig. 12. The two counter-propagating beams are made to overlap by overlapping the spots on the mirrors and the beam splitter. It is also important to make the beams pass accurately through the windows of the oven and the cell. By inserting BS4 and M4 the probe beam will be defined. It is important to choose a sufficiently small angle between the probe beam and the forward pump beam. As discussed in section A3, the spacing of the dominating grating increases for decreasing angle, and the relaxation phenomena become less noticeable. In the case of sodium the angle should not be larger than 1.5 degrees. If, for some reason, a larger angle is needed, it is always easier to start with a small one and increase it once the signal has been found found. The easiest way to estimate the angle is to observe the two spots on a white card inserted close to mirror M3.

The appropriate temperature for sodium is about 145°C in a 5 mm long cell and somewhat less in a longer cell.

We used a wavemeter to centre the laser within 0.1 Å of the

atomic transition. The signal should now be visible on a screen, which is placed before the photo diode, when scanning the laser over the transition.

If no signal is found take a closer look at the cell. When scanning the laser through the line centre, strong fluorescence should be seen in the cell. If this is not the case check the wavelength on the wavemeter and the temperature in the oven.

An additional aid in finding the signal is to set up a simple saturation spectroscopy experiment. This can be done by retroreflecting the probe beam back through the cell. This test works best with the pump beams blocked. The incoming probe beam will now be called the pump beam and the back reflected beam will be called the probe beam. The pump beam will be attenuated due to absorption. This will make the probe beam weaker than the pump beam. The probe beam will also be subjected to absorption. By scanning the laser and observing the intensity of the probe beam the Doppler profile will be observed. If the laser is tuned off resonance the two beams will interact with different velocity groups due to the Doppler effect. At the centre of the profile the beams interact with atoms that move perpendicular to the direction of the two beams. This means that the beams interact with the same velocity group of atoms. Since the strong pump beam transfers a considerable proportion of these atoms to the excited state, the probe beam will suffer less from absorption. This will be seen as a dip in the absorption profile at the line centre.

By observing this signal it is possible to tune the laser to the line centre where the DFWM signal is expected to appear. We can also obtain a good idea of where the DFWM signal will appear spatially since both signals are reflected in almost the same sense. The main difference is that the DFWM signal is phase conjugated. This difference will only be noticed if there are any phase-changing optical components, e.g. a lens, present between the cell and BS6.

The DFWM signal should now be found by optimizing the overlap of the beams.

B2.2 RESULTS

In this section I will show some spectra of the sodium D_2 line obtained with DFWM. The spectra will be analysed and compared with spectra from saturation spectroscopy. The measured dependence of the DFWM signal on temperature and pump-probe angle will be given. A comparison with theoretical dependences, as discussed above, will be made. A simple demonstration of the phase conjugated property of the reflected signal will conclude this section.

Fig. 13 shows a typical DFWM spectrum of the sodium D_2 line. The spectrum contains two lines corresponding to different hyperfine transitions. An energy level diagram is also included in the figure. This illustrates the hyperfine structure of the two states and indicates possible transitions. The reason why only two of these transitions are observed is optical hyperfine pumping in the ground state. If the laser is tuned to the F=2 to F=2 transition the atoms that have been excited will be given the chance to deexcite to either of the F=1 or the F=2 ground states, due to the transition rule $\Delta F=0,\pm1$. But once an atom has been transferred to the F=1 state it can not be excited by the laser. The long-term effect of the process is to transfer the F=2 atoms to the F=1

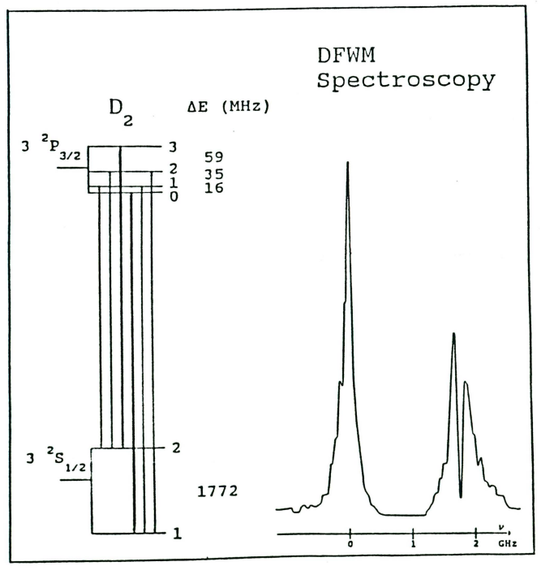

Fig. 13. A typical DFWM spectrum of the sodium D_2 line. This was obtain in a 5 mm long cell at a temperature of 160°C. The total power from the laser was 140 mW. The energy diagram shows the hyperfine structure of the D_2 line.

state. The F=2 ground state will be kept almost empty. Since no atoms are present in the F=2 ground state no DFWM signal can originate from this state. The only transitions that do not change the ground state equilibrium are the F=2 to F=3 and F=1 to F=0 transitions. These transitions form closed systems since the excited atoms can decay only to their original state. The signal corresponding to either of the transitions is a doublet due to Rabi splitting. This phenomenon was described in section A4.

Fig. 14 illustrates the difference between spectra obtained with DFWM and saturation spectroscopy. The latter was obtained by inserting a beam splitter in the backward pump beam. A small portion of the forward pump beam was split off and detected with a photodiode. Since this beam has passed through the cell it can be regarded as the signal in a saturation spectroscopy experiment. The DFWM signal and the saturation spectroscopy signal were fed to

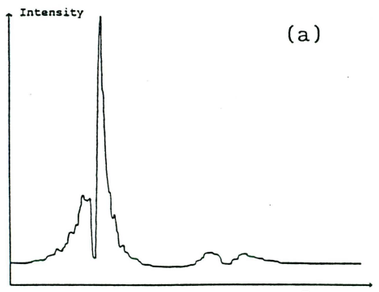

Fig. 14. Comparison between DFWM (a) and saturation spectroscopy (b). These spectra were obtained from a 8 cm long cell at a temperature of about 136°C. The total power from the laser was 700 mW.

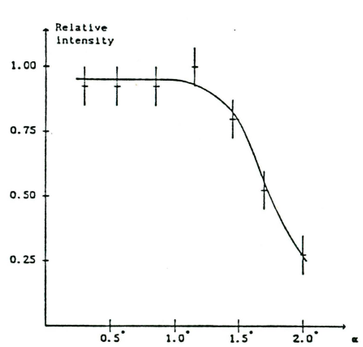

Fig. 15. Angle dependence of the DFWM signal. α is the angle between the probe and the forward pump beam. The temperature was 156°C in a 5 mm cell. The total power from the laser was 140 mW.

negative lens of focal length -10 cm followed by a positive lens of focal length 40 cm. This combination expanded the probe beam from its original diameter of 5 mm to 25 mm. This larger diameter made it easier to shape the beam profile to the desired pattern. The positive lens was placed approximately 40 cm after the f=-10 cm lens. This resulted in a focus approximately 2.5 metres after the f=40 cm lens. The cell was placed slightly in front of this point. The beam diameter was about 1 mm in the cell.

This set-up resulted in a spatially shaped signal. This signal was mixed with a background of scattered light. The background was suppressed by focusing the signal with a positive lens of short focal length and placing a small hole at the focus. Since the background was out of focus at this point only a small portion of it could pass through this filter. By using another positive lens the diverging beam was transformed to a parallel beam, which could be inspected on a white wall a few metres away. In order to illustrate the phase conjugating property of the process, the image was studied when the probe beam was distorted. This distortion was obtained by inserting a methanol flame in the beam. Fig. 17 (a) and (b) illustrate the probe image with and without the flame. The photographs were taken by allowing the probe beam to fall onto a white wall. The shutter was left open for about one second. When watching the object live on the wall a significant difference was observed between the two cases. The nondistorted probe beam resulted in a fixed picture on the wall whereas the distorted object was found to be moving about. This effect is due to refractive index variations in the flame. Since the shutter was left open for one second the photograph of the distorted probe appears diffuse. Will the signal resulting from these two different cases differ? Fig. 17 (c) and (d) give the answer as it appeared on the white wall. The camera was left open for about 10 seconds. I think that the pattern is just as sharp in both cases. The speckle pattern, which is undesired noise, tends to move about and disappears in the time integration. The pattern which is the image of interest was completely still on the wall. The phase distortion has served a purpose in discriminating uninteresting information.

C CONCLUSIONS

Degenerate four-wave mixing has recently proved to be an interesting method in many applications. In this paper I have tried to review some of the relevant theory and to perform some experiments which demonstrate the basic properties of the method.

One interesting application is found to be spectral and analytical investigations in hostile environments such as flames, where the phase conjugating property can be fully explored. This application is investigated in a following diploma project [22], where the method is extended into the low-concentration regime.

[21] D.G. Steel, R.C. Lind, J.F. Lam and C.R. Riuliano, Appl. Phys. Lett. **35**, 376 (1979).

[22] P. Bengtsson, Degenerate Four-Wave Mixing as a Analytical Tool, Lund Reports on Atomic Physics LRAP-99 (1989).